Available online at www.sciencedirect.com

ScienceDirect

Geochimica et Cosmochimica Acta 272 (2020) 121–136

Geochimica et Cosmochimica Acta

www.elsevier.com/locate/gca

Selenium isotope fractionation during adsorption by Fe, Mn and Al oxides

Wenpo Xu [a,b,c], Jian-Ming Zhu [b,*], Thomas M. Johnson [d,*], Xiangli Wang [e,f], Zhi-Qing Lin [g], Decan Tan [a,b,c], Haibo Qin [a]

[a] State Key Laboratory of Environmental Geochemistry, Institute of Geochemistry, Chinese Academy of Sciences, Guiyang 550081, China
[b] State Key Laboratory of Geological Processes and Mineral Resources, China University of Geosciences, Beijing 100083, China
[c] University of Chinese Academy of Sciences, Beijing 100049, China
[d] Department of Geology, University of Illinois at Urbana-Champaign, Urbana, IL 61801, USA
[e] Department of Marine Sciences, University of South Alabama, Mobile, AL 36688, USA
[f] Dauphin Island Sea Lab, Dauphin Island, AL 36528, USA
[g] Environmental Sciences Program and Department of Biological Sciences, Southern Illinois University, Edwardsville, IL 62026-1099, USA

Received 8 November 2018; accepted in revised form 2 January 2020; available online 7 January 2020

Abstract

Adsorption plays an important role in the biogeochemical cycling of selenium (Se) in natural environments and Se isotope fractionation during adsorption is a significant but poorly studied part of Se isotope system. This paper examined Se(IV) and Se(VI) adsorption onto four naturally occurring metal oxides (hematite, manganese dioxide (β-MnO_2), and α and γ-alumina oxides) and revealed Se isotope fractionation as a function of the absorbents used, Se species adsorbed, exposure time, and pH. The results show that Se(IV)/(VI) adsorption was initially rapid and was accompanied with kinetic isotope fractionations as large as 3‰, but slowed down as adsorption equilibrium was approached, eventually approaching isotopic equilibrium. The Se(IV) adsorption onto the studied metal oxides took at least 12 h to reach adsorption equilibrium, longer than Se (VI) adsorption (<60 min). At adsorption equilibrium, Se(IV) adsorption onto Fe and Mn oxides induces significant isotope fractionation, with lighter Se isotopes preferentially adsorbed, whereas Se(IV) adsorption onto Al oxides causes only small fractionation: $\Delta^{82/76}Se_{dissolved\text{-}adsorbed} = \delta^{82/76}Se_{dissolved} - \delta^{82/76}Se_{adsorbed}$ is 0.87 ± 0.12 ‰ for hematite, 1.24 ± 0.05 ‰ for β-MnO_2, 0.08 ± 0.10 ‰ for α-alumina, and 0.05 ± 0.09 ‰ for γ-alumina at pH 5. In contrast to Se(IV) adsorption, Se(VI) adsorption does not induce detectable Se isotope fractionation. The contrasting Se isotope fractionation between Se(IV) and Se(VI) adsorption is likely related to the mechanism of adsorption onto metal oxides, which causes a structural difference between dissolved and adsorbed Se(IV)/Se(VI). In addition, pH had a strong influence on Se isotope fractionation during Se (IV) adsorption onto β-MnO_2: $\Delta^{82/76}Se_{dissolved\text{-}adsorbed}$ varied from 1.24‰ to −0.08‰ as pH increased from 5 to 8. However, there was little pH effect on Se isotope fractionation during adsorption onto Fe (consistently at 0.7–0.9‰) and Al oxide (consistently at ~0‰). Our findings show that, beside abiotic and biotic reduction, Se(IV) adsorption onto Fe-Mn oxides is potentially another important process that can induce Se isotope fractionation in Earth's surface environments. This moves an important step toward correctly reconstructing the Se isotopic composition of seawater using Fe-Mn nodules or crusts.

Keywords: Se adsorption; Isotope fractionation; Hematite; Alumina; Manganese oxide

* Corresponding authors. Fax: 86-010-82322832 (J.-M. Zhu); 01-217-2444996 (T.M. Johnson).
E-mail addresses: jmzhu@cugb.edu.cn (J.-M. Zhu), tmjohnsn@illinois.edu (T.M. Johnson).

https://doi.org/10.1016/j.gca.2020.01.001
0016-7037/

1. INTRODUCTION

Selenium (Se) is a micronutrient and trace element that has drawn increasing attention due to not only its essential function in human and animals, but also is toxicity at high concentrations (WHO, 1987; Rayman, 2000). Selenium isotopes can serve as a useful proxy to track Se sources and redox processes, as well as to reconstruct the evolution of the biogeochemical Se cycle (Johnson et al., 1999, 2000; Rouxel et al., 2002, Mitchell et al., 2012; Zhu et al., 2014; Stüeken et al., 2015b, c; Pogge von Strandmann et al., 2015).

As a group VI element in the periodic table, Se is a redox-sensitive element. In natural environments, Se has four stable oxidation states: -II (selenide), 0 (elemental Se), IV (Se(IV), selenite/hydroselenite, SeO_3^{2-}/$HSeO_3^-$), and VI (selenate, SeO_4^{2-}) (Elrashidi et al., 1987; Johnson et al., 1999; Seby et al., 2001; Johnson and Bullen, 2004). Selenides can be found in soils, sediments, ore deposits, and organic Se compounds formed by assimilatory biological reduction of inorganic Se (Simon et al., 1997; Liu et al., 2000; Johnson, 2004; Johnson and Bullen, 2004; Zhu et al., 2004, 2012). Elemental Se is scarcely soluble (Johnson, 2004; Zhu et al., 2004, 2012), but it can be oxidized to bioavailable forms via hydrolyzation and microbial oxidation (McNeal and Balistrieri, 1989; Dowdle and Oremland, 1998). Selenite and hydroselenite are soluble, but adsorb strongly onto metal oxides, clay minerals, and organic matter. Selenate is highly soluble, mobile, bioavailable and without strong adsorption onto metal oxides compared to selenite (Balistrieri and Chao, 1990; Ellis et al., 2003; Johnson, 2004; Johnson and Bullen, 2004).

Because of the complex geochemistry of Se, Se isotope systematics are still not fully understood. Previous studies mainly focused on Se isotope fractionation during redox processes, with a range of −14.20 to 11.37‰ (Johnson et al., 1999; Rouxel et al., 2002; Herbel et al., 2002; Zhu et al., 2014); much less research has been done to investigate Se isotope fractionations related to other processes such as adsorption. Johnson et al. (1999) and Mitchell et al. (2013) found ≤0.8‰ Se isotope fractionation during adsorption of Se (IV)/Se (VI) onto iron oxides, with a wider range of adsorbents yet to be investigated. With the utilization of Se double spikes from the early 2000s (Johnson et al., 1999, 2000; Johnson and Bullen, 2003), one can now distinguish small Se isotope fractionations potentially induced by many previously unstudied processes. Insights about Se isotope fractionation during adsorption can be drawn from molybdenum (Mo) isotope fractionation. Barling and Anbar (2004) found that MoO_4^{2-} adsorption onto manganese oxide (MnO_2) induces 3.00 ± 0.15‰ fractionation, expressed as $\Delta^{98}Mo_{dissolved\text{-}adsorbed} = \delta^{98}Mo_{dissolved} - \delta^{98}Mo_{adsorbed}$. Goldberg et al. (2009) also observed that MoO_4^{2-} adsorption onto hydrous ferric oxide (HFO), goethite, and hematite caused significant isotope fractionations of 1.11 ± 0.15‰, 1.40 ± 0.48‰, and 2.19 ± 0.54‰, respectively. Considering similar ionic charge and molecular structures between Mo and Se oxyanions, Se oxyanion adsorption onto various absorbents, in the absence of redox reactions, may also result in distinguishable differences in Se isotopic compositions between adsorbed and dissolved phases.

Iron (Fe) and manganese (Mn) oxides are common in soils, sediments, and they are the major components of oceanic ferromanganese crusts and nodules (Bekker et al., 2010; Marcus et al., 2015) that could serve as good archives of seawater Se isotope composition through the Cenozoic. The common and representative Fe and Mn oxides are hematite and MnO_2, which have large surface areas and strong affinity to anions and cations (Saeki and Matsumoto, 1994; Pokrovsky et al., 2005). Both Se(VI) and Se(IV) can be adsorbed onto hematite, but the affinity for Se(VI) is much weaker than that for Se(IV) (Duc et al., 2006). This is likely due to the fact that Se (IV) adsorbed onto hematite mostly forms inner sphere complexes while Se(VI) tends to form outer-sphere complexes (Hayes et al., 1987a, b; Catalano et al., 2006b). Recent studies showed that different surface complexations can cause different isotope fractionations for B, Ni, Zn, Cd, Ge, Mo and W systems (Lemarchand et al., 2005, 2007; Pokrovsky et al., 2005, 2014; Kashiwabara et al., 2009, 2011, 2017; Li and Liu, 2010; Wasylenki et al., 2008, 2011, 2014; Gueguen et al., 2018). Therefore, we hypothesize that different adsorption mechanisms would result in different Se isotope fractionations. In contrast, Se(IV) is only adsorbed onto MnO_2 through inner-sphere complexation mechanisms (Balistrieri and Chao, 1990; Foster et al., 2003). To date, no data have been reported for Se isotope fractionation during Se(IV) and Se(VI) adsorption onto Mn oxides.

Aluminum (Al) oxides and hydroxides are widely distributed in soils, sediments and rocks. Peak (2006) and co-workers (Peak et al., 2006) carried out a series of experiments to reveal the adsorption mechanism of Se oxyanions onto different Al oxides and other minerals containing Al oxides. Based on X-ray Absorption Fine Structure (XAFS) data, they found that Se(IV) formed a mixture of outer-sphere and inner-sphere corner-sharing complexes on hydrous Al oxide, while Se(VI) formed inner-sphere mono-dentate complex on Al oxide at pH 4.5 and above. Although the mechanism for adsorption of Se oxyanions onto Al oxides have been explored in detail (Peak, 2006; Peak et al., 2006), the Se isotope fractionation during adsorption onto Al oxides has not yet been reported.

In this paper, we report an experimental investigation of Se isotope fractionation during adsorption onto hematite (α-Fe_2O_3), two aluminum oxides (α-Al_2O_3 and γ-Al_2O_3) and manganese dioxide (β-MnO_2; pyrolusite). The objectives are to investigate: (1) the magnitude of Se isotope fractionations between Se in solution and Se adsorbed onto Fe, Mn and Al oxides; and (2) the factors affecting Se isotope fractionation during adsorption (Se speciation, adsorbents, and pH); (3) possible fractionation mechanisms and the implications for using the Se isotope system to reconstruct paleo-seawater and to track Se pollutants.

2. MATERIALS AND METHODS

2.1. Mineral and Se solution preparation

Hematite (α-Fe_2O_3), aluminum oxides (α-Al_2O_3 and γ-Al_2O_3), and manganese oxide (β-MnO_2) were purchased

from Alfa Aesar China (Shanghai, China). Before the adsorption experiments, metal oxides were pre-processed to eliminate possible Fe (II) that might be present in oxides, because Fe (II) can reduce Se oxyanions and induce >1‰ Se isotope fractionation (Johnson and Bullen, 2003). To eliminate Fe (II), metal oxides were placed in ceramic crucibles and baked inside a muffle furnace at 300 °C for 24 h, which can transform Fe (II) to Fe (III) but without phase-transition of original metal oxides. Finally, all metal oxides were determined via XRD to confirm there was no structural change. Surface areas were subsequently measured by the multipoint BET (Brunauer–Emmett–Teller) method. The surface area was 23.6 m^2/g for hematite, 2.2 m^2/g for β-MnO_2, 10.6 m^2/g for α-Al_2O_3, 33.6 m^2/g for γ-Al_2O_3 and 20.6 m^2/g for the mixture of hematite and β-MnO_2.

The Se stock solutions were prepared by dissolving sodium Se(IV) (Na_2SeO_3) and sodium Se(VI) (Na_2SeO_4) salts obtained from Alfa Aesar China in O_2-free (N_2 purged) ultrapure water (18.2 MΩ). Then 0.1 mol/L HCl and NaOH were used to adjust the pH of the Se stock solution to be 5, 6, 7, and 8. pH-adjusted stock solutions were purged with high purity N_2 for 20 min to remove dissolved oxygen and carbon dioxide. Stock solutions as well as experimental samples were stored at 4 °C until Se concentrations were measured by hydride generation atomic fluorescence spectrometry (HG-AFS).

2.2. Adsorption experiment

The matrix for all of the adsorption experiments was 0.1 mol/L NaCl (GR). The metal oxides were added into the 0.1 mol/L NaCl solution to form 1.5 g/L suspensions (except for MnO_2, which was 3 g/L). For the time series experiments, the pH of the suspension solution was adjusted to 5.0 with 0.1 M HCl and NaOH. The suspension pH was re-adjusted 30 min after mixing and the suspension solution was purged with ultrapure nitrogen gas for 15 min. The serum bottles (125 mL) were crimp-sealed and placed on a shaker at 120 rpm and 22 ± 2 °C. The Na_2SeO_3 or Na_2SeO_4 solution was injected into the serum bottles to start each experiment. Initial Se concentrations were selected based on the adsorption capacity of the metal oxides. The initial Se concentrations for Se(IV) adsorption on hematite, MnO_2, α-Al_2O_3, and γ-Al_2O_3 were 10, 1.25, 2.0, and 2.5 mg/L, respectively. For Se(VI) adsorption, the initial Se concentration was fixed at 1.0 mg/L.

At each sampling time, 2 mL suspension was taken from each experimental bottle using a syringe, filtered through a 0.22 μm polysulfone membrane filter, and stored in high density polyethylene (HDPE) conical centrifuge tubes. Meanwhile, the same volume of N_2 gas (i.e., 2 mL) was injected into each bottle. The solid phase materials were washed for 3–5 times using O_2-free ultrapure water to remove dissolved Se remaining on the metal oxides, then dissolved in 5 mol/L HCl and stored at 4 °C. Samples were collected at 0, 1, 4, 7, 10, 20, 30 min, and 1 hour, and then 3, 6, 12, 24, 48, and 72 h.

Because pH strongly affects the adsorption process (Hayes et al., 1987a, b; Peak, 2006), a series of different pH experiments were carried out at pH = 5, 6, 7, and 8 to cover the pH range of river water, seawater, and soil (Barling and Anbar, 2004). Previous studies have shown that the adsorption equilibrium on Fe, Mn and Al oxides can be reached in 24 h (Balistrieri and Chao, 1990; Kuan et al., 1998; Johnson et al., 1999; Catalano et al., 2006b; Peak, 2006; Duc et al., 2006; Mitchell et al., 2013). To ensure isotopic equilibrium was reached, several samples were also taken after 3 days, following procedures as described above.

In addition, hematite and MnO_2 were also mixed at a Fe-Mn mass ratio of 1:1 to simulate the oxides commonly found in sediments and evaluate the effect of ternary systems on Se isotope fractionation. This experiment was carried out following the same procedures described above, except that the initial Se(IV) concentration was fixed at 5 mg/L.

2.3. Sample preparation and separation

2.3.1. Se concentration analysis

Concentrations of total Se were measured by Atomic Fluorescence Spectroscopy (AFS) equipped with a continuous flow hydride generator (HG) system and a boosted discharge hollow cathode Se lamp. A mixture of 0.2% sodium hydroxide (NaOH) and 1.5% potassium borohydride (KBH_4) (m/m) was used as the reduction reagent (Zhu et al., 2008, 2014). Calibration standards were prepared in 6% HCl (v/v) with concentrations ranging from 2 to 20 mg/L. The relative standard deviation (RSD) of the Se standard solution measurements was approximately 5%. Because the hydride generation method only measures Se in the form of Se(IV), for the Se(IV) adsorption experiments, Se concentrations were determined directly by HG-AFS after diluting a small aliquot (100 μL of the filtrate samples) with 6% HCl. For the Se(VI) adsorption experiments, Se(VI) was converted to Se(IV) prior to measurement. 100 μL aliquot samples were added to 25 mL borosilicate glass tubes with Teflon-lined caps filled with 3 mL 5 mol/L HCl. The solution was then heated at 100 °C for about 55 min, diluted to 6% HCl with ultrapure-water, and cooled prior to Se measurement with HG-AFS or HG-MC-ICPMS (Zhu et al., 2008, 2014).

To determine if Se(IV) was transformed to Se(VI) during Se(IV) adsorption onto metal oxides, two 0.1 mL aliquots were sampled after 360 h. One aliquot was mixed with 6% HCl for direct Se analysis, and the other was added to 5 mol/L HCl and heated for 55 min to reduce Se(VI) to Se(IV) prior to the chemical analysis. No significant difference between the two analyses was observed, indicating that no Se(VI) was formed during the experiments.

2.3.2. Purification of Se

Anion exchange resin column AG1-X8 (100–200 mesh) was used to separate Se from the solute matrix components, including interfering elements such as Fe. Before the sample purification, a double isotope spike containing ^{74}Se and ^{77}Se with a known $^{77}Se/^{74}Se$ ratio was added to, and equilibrated with samples to correct for the isotopic fractionation occurring during Se purification and mass

spectrometry (Johnson et al., 1999; Zhu et al., 2008, 2014). The ratio of spike to sample ($^{77}Se_{spike}/^{78}Se_{sample}$) was 2 according to an earlier study by Zhu et al. (2008). Detailed purification procedures were modified from Ellis et al. (2003) and Zhu et al. (2008, 2014). Briefly, samples containing ~100 ng Se were added into 15 mL PFA beakers, mixed with double spike in 1 mL concentrated nitric acid, and allowed to equilibrate over night. The PFA beakers were then placed on a hot plate at 90 °C to evaporate samples to incipient dryness. Then 1 mL 0.03 mol/L potassium persulfate ($K_2S_2O_8$) was added into the beaker followed by heating on a plate at 130 °C for 2 h with caps closed, to convert all Se to Se(VI). Meanwhile, the anion exchange resin AG1-X8 was washed with 10 mL 6 mol/L HCl, and then rinsed with ultrapure water until the pH of the leachate from the resin became neutral. The resin columns were loaded with sample solutions, and were washed with 5 mL ultrapure water and 5 mL 0.1 mol/L HCl to remove possible interference elements As and Ge. Finally, Selenium (VI) was released from the resin with 5 ml 5 mol/L HCl and collected into 25 mL borosilicate glass tubes. The concentrated HCl (~0.7 mL) was then added into the tubes to ensure the solution contained 5 mol/L HCl. The tubes were then capped and heated to convert Se(VI) to Se(IV) as described above. After samples were cooled, high purity N_2 was used to purge through the sample solutions for 10–15 min to remove possible volatile Br species. The sample solutions were then diluted to attain a final HCl concentration of 2.0 ± 0.1 mol/L for Se isotope measurement.

2.4. Mass spectrometry and Se isotopes analysis

Selenium isotope analysis was carried out on a Multi-collector Inductively Coupled Plasma Mass Spectrometer (MC-ICP-MS) (Nu Plasma II, North Wales, UK) housed in the State Key Lab of Environmental Geochemistry at Institute of Geochemistry, Chinese Academy of Sciences, Guiyang, China. The MC-ICP-MS was equipped with 16 Faraday cups and 5 ion counters. Hydride generation was used as the sample introduction method: Se was introduced into the MC-ICP-MS as SeH_2 via an on-line continuous-flow hydride generator (HG). In this study, a mixture of 0.3% $NaBH_4$ and 0.4% NaOH was used as the reductant (Zhu et al., 2008). The sample and the reductant solutions were introduced into the HG system at a flow rate of 0.70 mL/min and 0.35 mL/min, respectively.

Selenium has six stable isotopes in nature, ^{74}Se, ^{76}Se, ^{77}Se, ^{78}Se, ^{80}Se and ^{82}Se with abundances 0.889%, 9.366%, 7.635%, 23.772%, 49.607%, and 8.731%, respectively. The 6 stable Se isotopes were simultaneously measured using the Faraday cups of H8, H6, H2, Ax, L2 and L4, respectively. Accuracy can be compromised by the presence of As and Br that form polyatomic interferences with H^+, and Ge that is a direct isobaric interference. To monitor and correct these interferences, ^{73}Ge, ^{75}As, and ^{79}Br were monitored via the ion counter IC2 and the Faraday cups of L4 and H4, respectively. To correct the interferences and obtain the ratios of $^{82}Se/^{76}Se$, $^{82}Se/^{78}Se$ and $^{78}Se/^{76}Se$, an iterative calculation routine was used to reduce data for each measurement cycle following a previous algorithm (Clark and Johnson, 2008; Zhu et al., 2008, 2014).

The Se isotope analysis quality control included a Se isotope standard reference material (NIST SRM 3149, $\delta^{82/76}Se_{SRM3149} = 0.00 \pm 0.10$ ‰) and an inter-laboratory quality control standard MH495 ($\delta^{82/76}Se_{MH495\text{-}SRM3149} = -3.44 \pm 0.10$‰) obtained from the Department of Geology, University of Illinois at Urbana-Champaign, Illinois, USA (Johnson et al., 1999, 2000; Zhu et al., 2008, 2014). Samples were introduced into the hydride generator at a concentration of 5–7 μg/L to produce 1.5–2.5 V ^{78}Se, which was a compromise between good counting statistics (high concentration) and easy washing of the sample introduction system (low concentration). To achieve normal and stable background signals and to avoid memory effects between samples, the hydride generator was rinsed with c.a. 2 mol/L HCl until a stable baseline signal was obtained. Prior to each sample measurement, on-mass baseline was measured and subtracted from the intensities obtained for each sample measurement cycle, prior to the data reduction calculations. In addition, NIST SRM 3149 was measured approximately every 3–5 samples to monitor the stability of the instrument. All isotopic ratios are expressed using the standard delta notation (Eq. (1)): per mil (‰) deviation of sample $^{82/76}Se$ ratio from the NIST SRM 3149 standard:

$$\delta^{82/76}Se = \left[\left(^{82/76}Se_{sample}/^{82/76}Se_{standard}\right) - 1\right] \times 1000 \quad (1)$$

The long-term $\delta^{82/76}Se$ value of NIST SRM 3149 that measured based on 2-standard deviation was 0.00 ± 0.10‰ (n = 96, 2SD) during a 24-month period. The $\delta^{82/76}Se$ of the secondary standard and Se stock solutions were measured to be −3.45 ± 0.10‰ (n = 45, 2SD) for MH495, −1.18 ± 0.12‰ (n = 12, 2SD) for Na_2SeO_3, and −0.50 ± 0.10‰ (n = 12, 2SD) for Na_2SeO_4.

The $\delta^{82/76}Se$ of the adsorbed Se (for the MnO_2 and the mixture of Fe and Mn oxides experiments) can be calculated using the mass balance equation (Eq. (2)):

$$\delta^{82/76}Se_{adsorbed} = \left(\delta^{82/76}Se_{stock} - \delta^{82/76}Se_{dissolved} \times f\right)/(1 - f) \quad (2)$$

where $\delta^{82/76}Se_{adsorbed}$, $\delta^{82/76}Se_{stock}$, and $\delta^{82/76}Se_{dissolved}$ represent the $\delta^{82/76}Se$ of the adsorbed Se, stock solution and Se remaining in solution, and *f* was the fraction of Se retained in solution. The errors of calculated $\delta^{82/76}Se_{adsorbed}$ is <0.2‰ (2SD). The equilibrium isotope fractionation during adsorption can be expressed as the difference in $\delta^{82/76}Se$ between adsorbed and dissolved Se at isotopic equilibrium:

$$\Delta^{82/76}Se_{dissolved-adsorbed} \approx \delta^{82/76}Se_{dissolved} - \delta^{82/76}Se_{adsorbed} \quad (3)$$

3. RESULTS

3.1. The adsorption behavior of Se oxyanions

In order to quantify these experimental observations, we calculated the amount of Se oxyanions adsorbed onto metal oxides in milligram (mg) per gram (g) using the mass balance equation:

$$Q_t = (C_0 - C_t) * V/m \quad (4)$$

where Q_t (mg/g) is the adsorbed Se concentration at time t (h), C_0 (mg/L) and C_t (mg/L) are Se dissolved concentrations at 0 h and t hour, respectively, V is the volume of solution (L) and m is the mass (g) of the adsorbents.

Fe and Al oxides rapidly adsorbed Se(VI) and adsorption equilibrium was reached within 60 min (Fig. 1B, 1F and 1H). In contrast, β-MnO_2 didn't adsorb Se(VI) significantly. In comparison with Se(VI), adsorption of Se(IV) onto all four selected metal oxides (hematite, manganese oxides, alumina) took at least 12 h to reach the adsorption

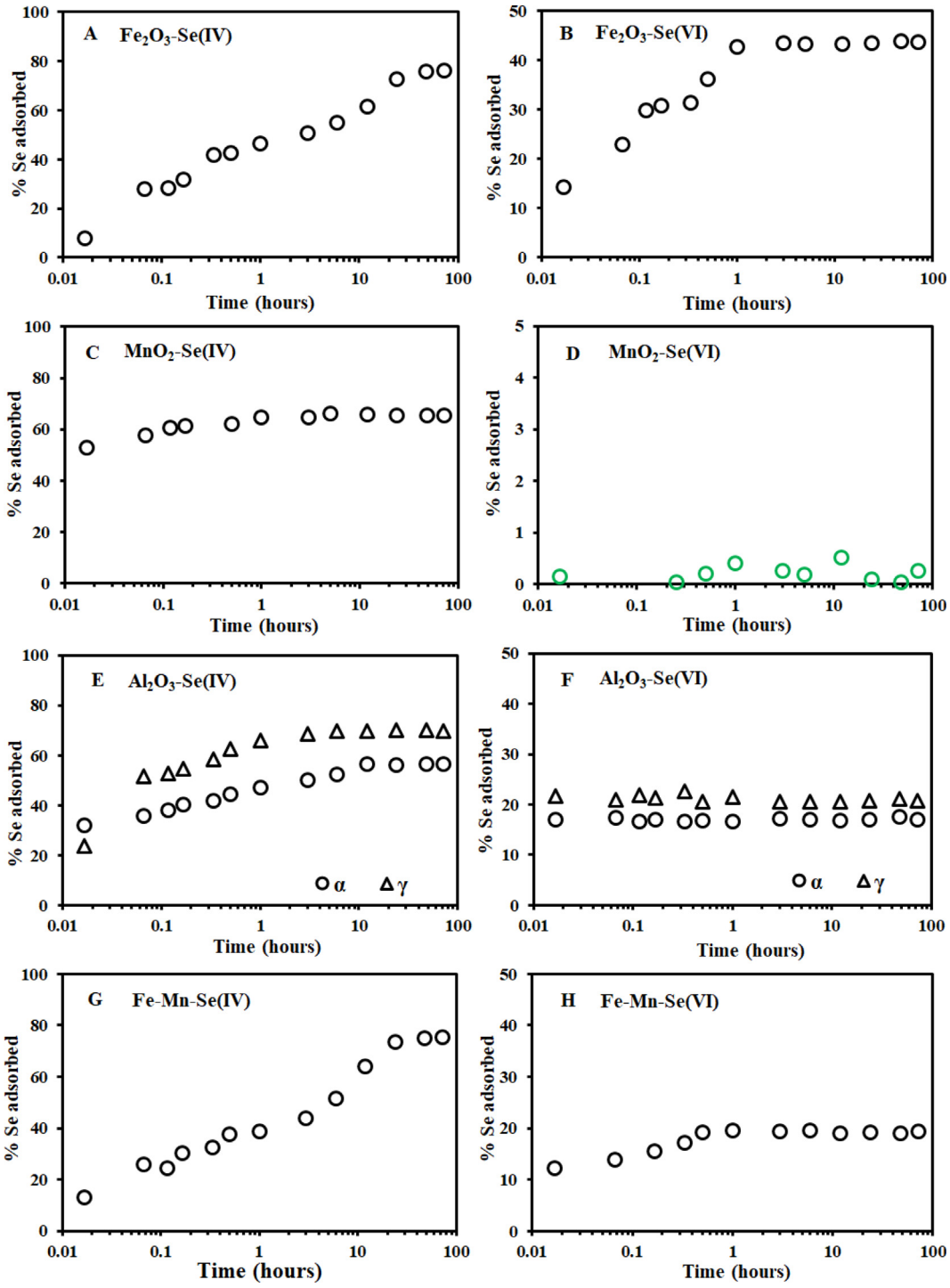

Fig. 1. Se (IV) (left) and Se (VI) (right) adsorption onto Fe, Mn and Al oxides as a function of time at pH = 5. α: α-Al_2O_3; γ: γ-Al_2O_3. Green symbol represents % Se adsorbed onto MnO_2. (For interpretation of the references to color in this figure legend, the reader is referred to the web version of this article.)

equilibrium (Fig. 1A, C, E and G). In Se(IV) adsorption experiments, the adsorption capacity (Q_t at adsorption equilibrium) decreased in the order of hematite (4.68 mg/g) > Fe-Mn oxides mixture (2.36 mg/g) > γ-alumina (1.20 mg/g) > α-alumina (0.75 mg/g) > β-MnO_2 (0.27 mg/g). For Se(VI) adsorption experiments, the adsorption capacity order was hematite (0.38 mg/g) > γ-alumina (0.20 mg/g) > Fe-Mn oxides mixture (0.17 mg/g) > α-alumina (0.15 mg/g) > β-MnO_2 (~0 mg/g) (Fig. 1). In terms of surface area, the adsorption capacities of Se (IV) and Se(VI) were 198 and 16 μg/m^2 for hematite, 123 and 0 μg/m^2 for β-MnO_2, 71 and 14 μg/m^2 for a-alumina, and 36 and 6 μg/m^2 for γ-alumina, respectively.

3.2. Se isotope fractionation during adsorption

The measured $\delta^{82/76}$Se values of dissolved and adsorbed Se as a function of time are shown in Fig. 2. Note that the $\delta^{82/76}$Se values of Se adsorbed onto Mn oxides and Fe-Mn oxides were calculated based on mass balance.

In hematite adsorption experiments, lighter Se isotopes were preferentially adsorbed, enriching heavier Se isotopes in the solutions (Fig. 2A and B; Tables 1 and 2). It is clear that transient kinetic effects occurred in the first 30 min of the experiments, but isotopic values stabilized after about 24 h, suggesting that isotopic equilibrium had been attained. For example, adsorption of Se(IV) induced ~3‰ fractionation during the first initial 30 min, but the fractionation decreased to only 0.94‰ after 24 h, and eventually stabilized at around 0.87 ± 0.12‰ (Fig. 2A). The isotopic fractionation was not pH-dependent for hematite. Although the amount of adsorbed Se(IV) decreased with increasing pH, the $\Delta^{82/76}Se_{dissolved\text{-}adsorbed}$ did not vary significantly, ranging from 0.67‰ to 0.88‰ (Table 2). Based on average $\delta^{82/76}$Se values after isotopic equilibrium was attained the experiments yielded $\Delta^{82/76}Se_{dissolved\text{-}adsorbed}$ values of 0.87 ± 0.12‰ (2SD) for Se(IV), and 0.22 ± 0.06‰ (2SD) for Se(VI) at pH = 5.

During Se (VI) adsorption onto β-MnO_2 (Fig. 2D), the $\delta^{82/76}$Se value of the dissolved Se was close to the stock solution throughout the experiment, consistent with the observation that there was no adsorption as shown in Fig. 1D. In the experiment with Se(IV) and β-MnO_2 (Fig. 2C), the $\delta^{82/76}$Se of the dissolved Se increased initially from −1.18‰ to −0.03‰, but decreased to −0.34‰ as it reached adsorption equilibrium. The final $\Delta^{82/76}Se_{dissolved\text{-}adsorbed}$ was 1.24‰, indicating that the lighter Se isotopes were preferentially adsorbed onto β-MnO_2. However, pH had a great effect on Se isotope fractionation during Se(IV) adsorption onto β-MnO_2, with the $\Delta^{82/76}Se_{dissolved\text{-}adsorbed}$ decreasing strongly from 1.24‰ at pH 5 to −0.08‰ at pH 8 (Table 2).

In the pH 5.0 experiments with Se(IV) and α- and γ-alumina, the $\delta^{82/76}$Se values of the dissolved Se at adsorption equilibrium (after 48 hour) were −1.16 ± 0.05‰ and −1.21 ± 0.05‰, respectively, equal to the stock solution, within the analytical uncertainties (Fig. 2E and G). The $\Delta^{82/76}Se_{dissolved\text{-}adsorbed}$ was 0.08 ± 0.10 ‰ for α-alumina and 0.05 ± 0.09 ‰ for γ-alumina, indicating that there was little or no equilibrium isotope fractionation, despite significant adsorptions (Fig. 1E). Similar results were obtained at all pH values tested. However, a transient kinetic effect was observed: The $\delta^{82/76}$Se values of dissolved Se(IV) increased from −1.18‰ to −0.05‰ in the initial 30 min and then decreased back to −1.13‰ after 24 h for α-alumina, and from −1.18‰ to −0.33‰ in the initial 30 min then decreased to −1.23‰ after 24 h for γ-alumina (Fig. 2E and G). In the experiments with Se(VI) and α-alumina and γ-alumina, the $\delta^{82/76}$Se values of dissolved Se at equilibrium were not significantly different from the stock solution, indicating that there was little or no Se isotope fractionation. Also, the $\delta^{82/76}$Se values of dissolved Se (VI) didn't change over time in the early stages of the experiments.

In the experiment of Se adsorption onto mixed Fe-Mn oxides, the $\delta^{82/76}$Se values of dissolved Se changed over time like the experiments of Se adsorption onto hematite and MnO_2 (Fig. 2 and J, Table 1). For Se(IV) adsorption, the $\Delta^{82/76}Se_{dissolved\text{-}adsorbed}$ values was 1.15‰ at adsorption equilibrium, falling in between hematite and β-MnO_2 (Fig. 2I; Table 1). For Se(VI) adsorption, the $\delta^{82/76}$Se values were close to the starting solution value, and the $\Delta^{82/76}Se_{dissolved\text{-}adsorbed}$ was < 0.10 ‰, indicating no significant Se isotope fractionation (Fig. 2J; Table 1).

4. DISCUSSION

4.1. The adsorption mechanism of Se(IV) and Se(VI)

In this study, the maximum adsorption of Se (IV) onto Fe, Mn, and Al oxides was significantly larger than that of Se(VI). These observations are consistent with previous studies and confirm that the selected four metal oxides have stronger affinity to Se(IV) than Se(VI) (Hayes et al., 1987a, b; Balistrieri and Chao, 1990; Zhang and Sparks, 1990; Saeki and Matsumoto, 1994; Saeki et al., 1995; Peak, 2006; Rovira et al., 2008; Mitchell et al., 2013). Meanwhile, the equilibration time of Se(IV) adsorption was longer than that of Se(VI) adsorption (Fig. 1), especially during Se(IV) adsorption onto hematite and Fe-Mn oxide. This suggests that the mechanisms of Se(IV) and Se(VI) adsorption onto these metal oxides are different. Previous studies suggested that outer-sphere complexes should reach equilibrium within a few minutes, whereas inner-sphere complexation is expected to be much slower because old bonds are broken, and new ones are formed (Hayes et al., 1987a, b; Zhang and Sparks, 1990; Foster et al., 2003; Catalano et al., 2006b; Peak, 2006; Duc et al., 2006). These studies proposed that metal oxides could form Me-OH functional groups in contact with the solution and might have the following reactions with Se oxyanions:

(a) Se (IV) adsorption (outer-sphere)

$$\text{Me-OH} + 2H^+ + SeO_3^{2-} \rightleftharpoons MeOH_2^+\text{-}(HSeO_3)^- \quad (5)$$

(b) Se (IV) adsorption (inner-sphere)

$$\text{Me-OH} + H^+ + SeO_3^{2-} \rightleftharpoons Me(SeO_3)^- + H_2O \quad (6)$$

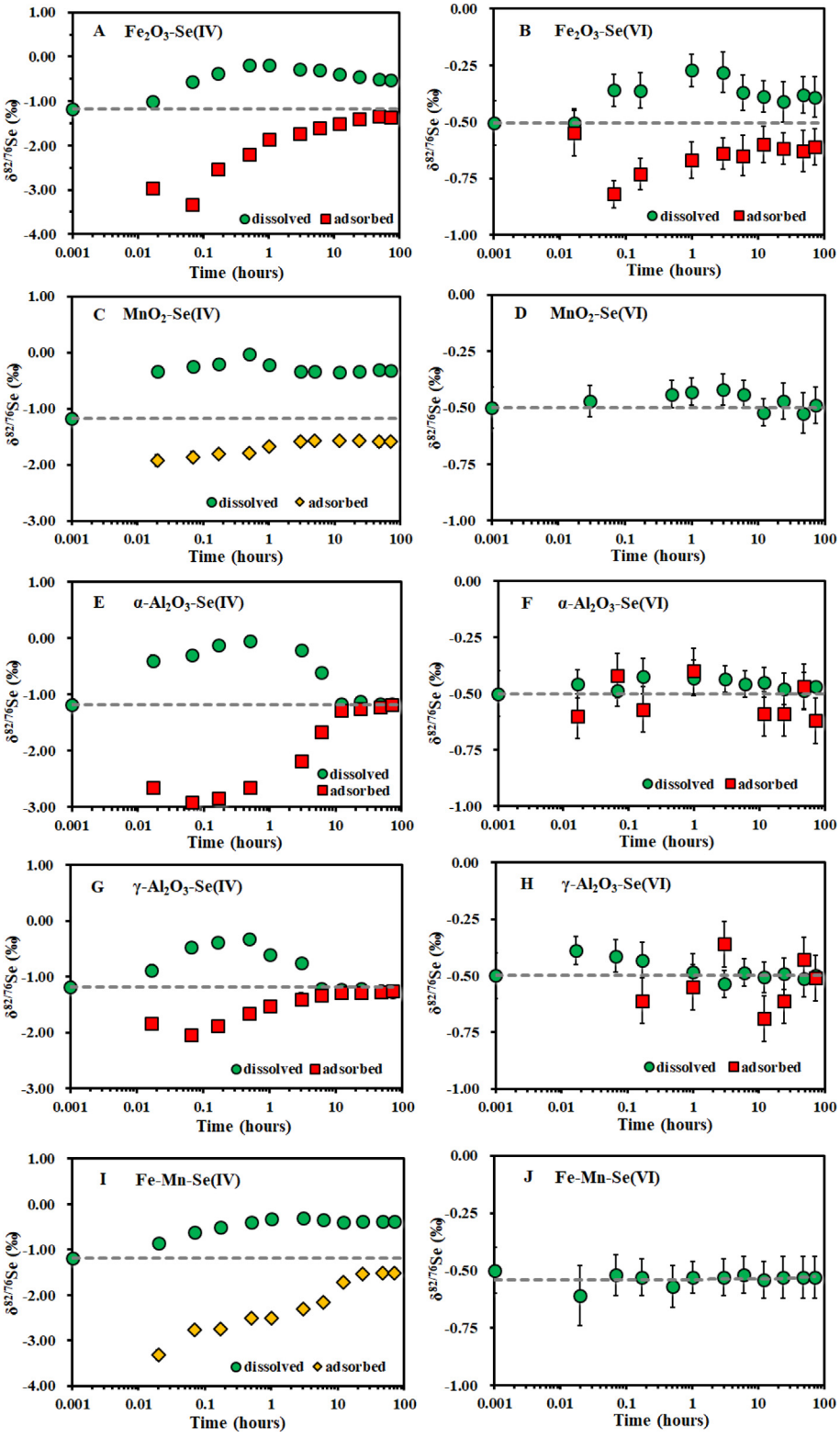

Fig. 2. $\delta^{82/76}$Se values of dissolved (green circle) and adsorbed (red circle) Se over time at pH = 5. Yellow diamonds represent calculated $\delta^{82/76}$Se values for Se adsorbed onto solids (measurements were not made). Adsorbed Se isotope data in D and J were not shown because lack of isotope fractionation. Grey dashed lines represent the $\delta^{82/76}$Se values of the stock solutions. (For interpretation of the references to color in this figure legend, the reader is referred to the web version of this article.)

Table 1
Results for Se anions adsorption onto Fe, Mn, and Al oxides at pH 5.

Se valence	Adsorbents	f[1]	$\delta^{82/76}Se_{dissolved}$	$\delta^{82/76}Se_{adsorbed}$	Mass balance[3] (‰)	$\Delta^{82/76}Se$	Uncertainty of Δ
Se(IV)	α-Fe_2O_3	0.24	−0.52	−1.39	−1.17	0.87	0.12
	β-MnO_2	0.32	−0.32	−1.56[2]	−1.16	1.24	0.05
	α-Al_2O_3	0.44	−1.16	−1.22	−1.19	0.08	0.10
	γ-Al_2O_3	0.28	−1.24	−1.28	−1.27	0.05	0.09
	Fe-Mn oxide	0.29	−0.37	−1.52[2]	−1.19	1.15	0.02
Se(VI)	α-Fe_2O_3	0.57	−0.39	−0.61	−0.48	0.22	0.06
	β-MnO_2	1.00	−0.47	–	−0.47	–	–
	α-Al_2O_3	0.78	−0.47	−0.54	−0.49	0.08	0.09
	γ-Al_2O_3	0.73	−0.50	−0.53	−0.51	0.04	0.13
	Fe-Mn oxide	0.81	−0.51	−0.47[2]	−0.50	−0.03	0.32

[1] Fraction of Se remaining in solution.
[2] $\delta^{82/76}Se_{solid}$ is calculated by mass balance.
[3] $\delta^{82/76}Se$ of the bulk experiment calculated as $f(Se)*\delta^{82/76}Se_{dissolved} + (1\text{-}f(Se))*\delta^{82/76}Se_{adsorbed}$. Should equal $\delta^{82/76}Se$ of the stock Se solution.

Table 2
Results for Se(IV) sorption onto Fe, Mn, and Al oxides at different pH.

Adsorbents	$pH_{initial}$	pH_{final}	f[1]	$\delta^{82/76}Se_{dissolved}$	$\delta^{82/76}Se_{adsorbed}$	Mass balance[3] (‰)	$\Delta^{82/76}Se$	Uncertainty of Δ
α-Fe_2O_3	5*	6.65	0.41	−0.66	−1.54	−1.17	0.87	0.12
	6	6.76	0.52	−0.81	−1.58	−1.18	0.76	0.10
	7	6.86	0.63	−0.93	−1.60	−1.19	0.67	0.09
	8	6.78	0.73	−0.94	−1.81	−1.17	0.87	0.11
β-MnO_2	5	6.12	0.32	−0.32	−1.56[2]	−1.16	1.24	0.05
	6	6.56	0.65	−0.93	−1.65[2]	−1.18	0.72	0.10
	7	6.84	0.79	−1.12	−1.39[2]	−1.18	0.26	0.14
	8	6.89	0.87	−1.19	−1.11[2]	−1.18	−0.08	0.23
α-Al_2O_3	5	5.43	0.44	−1.16	−1.22	−1.19	0.08	0.10
	6	6.12	0.55	−1.19	−1.17	−1.18	−0.02	0.08
	7	6.74	0.73	−1.17	−1.20	−1.17	0.03	0.10
	8	7.17	0.88	−1.17	−1.22	−1.18	0.05	0.12
γ-Al_2O_3	5	5.65	0.28	−1.24	−1.28	−1.27	0.05	0.09
	6	6.23	0.50	−1.15	−1.22	−1.19	0.07	0.10
	7	6.83	0.67	−1.17	−1.20	−1.18	0.03	0.09
	8	7.12	0.81	−1.19	−1.10	−1.17	−0.10	0.12

* Parallel experiment.
[1] Fraction of Se remaining in solution.
[2] $\delta^{82/76}Se_{solid}$ is calculated by mass balance.
[3] $\delta^{82/76}Se$ of the bulk experiment calculated as $f(Se)*\delta^{82/76}Se_{dissolved} + (1\text{-}f(Se))*\delta^{82/76}Se_{adsorbed}$. Should equal $\delta^{82/76}Se$ of the stock Se solution.

$$Me\text{-}OH + 2H^+ + SeO_3^{2-} \rightleftharpoons MeHSeO_3 + H_2O \quad (7)$$

(c) Se (VI) adsorption (outer-sphere)

$$Me\text{-}OH + H^+ + SeO_4^{2-} \rightleftharpoons MeOH_2^+\text{-}(SeO_4)^{2-} \quad (8)$$

$$Me\text{-}OH + 2H^+ + SeO_4^{2-} \rightleftharpoons MeOH_2^+\text{-}(HSeO_4)^- \quad (9)$$

(d) Se (VI) adsorption (inner-sphere)

$$Me\text{-}OH + H^+ + SeO_4^{2-} \rightleftharpoons Me(SeO_4)^- + H_2O \quad (10)$$

A compilation of complex formation between Se oxyanions and oxide surfaces (Table 3) reveals that Se (IV) unambiguously forms strong inner-sphere complexes, whereas no definite conclusion has been reached regarding whether Se (VI) forms inner or outer-sphere complexes, even for experiments conducted at the same pH (Hayes et al., 1987a, b; Manceau and Charlet, 1994). Therefore, the mechanism of surface complex formation for Se (VI) seems complicated, and many factors should be considered such as pH, ionic strength and sample characteristics (wet or dry), etc. Fortunately, Se isotope fractionation might shed some light on the mechanism of Se (IV)/Se (VI) adsorption onto metal oxides. At pH 5, large Se isotope fractionation occurred during Se (IV) adsorption onto Fe and Mn oxides, whereas little or were no isotope fractionation (at adsorption equilibrium) was observed for Se (VI) adsorption onto Fe, Mn, and Al oxides, and for Se(IV) adsorption to Al oxides (Fig. 2). These results indicate that, at pH 5, inner-sphere surface complexes are formed during Se (IV) adsorption to Fe and Mn oxides, and outer-sphere surface complexes

Table 3
A summary of the complexes formation formed during Se oxyanions adsorption onto metal oxides.

Valences	Adsorbents	Types of surface complex	Method	Authors
Se(IV)	Goethite	inner-sphere	TLM/EXAFS	Hayes et al., 1987a, 1987b
	HFO	inner-sphere	TLM	Hayes et al., 1987a
		inner-sphere, binuclear	TLM	Balistrieri and Chao, 1990
	hematite	inner-sphere (monodentate or bidentate)	CCM	Duc et al., 2006
		inner-sphere	XSW	Catalano et al., 2006b
	manganese dioxide	inner-sphere, monodentate	TLM	Balistrieri and Chao, 1990
	K-birnessite	inner-sphere	EXAFS	Foster et al., 2003
	δ-MnO_2	inner-sphere	EXAFS	Foster et al., 2003
	hydrous aluminum oxide	a mixture of outer and inner-sphere	EXAFS	Peak, 2006
Se(VI)	Goethite	outer-sphere	TLM/EXAFS	Hayes et al., 1987a, 1987b
		inner-sphere	EXAFS	Manceau and Charlet, 1994
		inner-sphere (predominantly), monodentate, pH < 6 outer-sphere (predominantly), pH > 6	Raman and ATR-FTIR	Wijnja and Schulthess, 2000
		a mixture of outer and inner-sphere	EXAFS and ATR-FTIR	Peak and Sparks, 2002
	HFO	outer-sphere	TLM	Hayes et al., 1987a
		inner-sphere	EXAFS	Manceau and Charlet, 1994
		a mixture of outer and inner-sphere	EXAFS and ATR-FTIR	Peak and Sparks, 2002
		outer-sphere, monodentate	TLM	Balistrieri and Chao, 1990
	hematite	inner-sphere	EXAFS and ATR-FTIR	Peak and Sparks, 2002
	corundum (α-Al_2O_3)	pH = 3.5, outer-sphere pH ≥ 4.5, inner-sphere monodentate	EXAFS	Peak, 2006
	γ-Al_2O_3	outer-sphere (predominantly), pH > 6	Raman and ATR-FTIR	Wijnja and Schulthess, 2000
		outer-sphere(major) + inner-sphere (small), pH < 6		

Note: amorphous iron oxyhydroxide (HFO), Extended X-ray absorption fine structure (EXAFS), X-ray standing wave (XSW), Constant Capacitance Model (CCM), Triple layer model (TLM), Attenuated total reflectance-Fourier transform infrared spectroscopy (ATR-FTIR).

are formed during Se(IV) adsorption onto Al oxides and during Se (VI) adsorption onto Fe, Mn, and Al oxides. As pH increases, however, the $\Delta^{82/76}Se_{dissolved\text{-}adsorbed}$ for Se(IV) adsorption to β-MnO_2 decreases to ~0‰, suggesting that the formation of inner vs outer-sphere complexes between Se (IV) and β-MnO_2 depends on pH. For α- and γ-alumina, equilibrium Se isotope fractionation is consistently near zero at all pH values, suggesting that outer-sphere complexation is predominant.

4.2. The effect of Se speciation on Se adsorption and isotope fractionation

Se(IV)(e.g., SeO_3^{2-}, $HSeO_3^-$) and Se(VI) (e.g., SeO_4^{2-})are the predominant Se species in the aquatic environment (Elrashidi et al., 1987; Johnson and Bullen, 2004). Se speciation not only affects Se affinity to metal oxides, but also Se isotope fractionation during adsorption of Se oxyanions onto oxides (Figs. 1 and 2, Table 1). The isotope fractionation at Se (IV) adsorption equilibrium was generally larger than that at Se(VI) adsorption equilibrium. In addition, the isotopic equilibrium was attained slowly (more than 12 h) in the Se(IV) adsorption experiment than Se(VI) adsorption experiments (less than 1 hour). Se(IV) has three Se-O bonds arranged in a pyramidal oxyanion structure, whereas Se (VI) has four Se-O bonds arranged in a tetrahedral oxyanion structure (Peak, 2006). The Se-O bond length in Se(IV) is ~1.70 Å, while that of Se(VI) is ~1.65 Å. Therefore, the Se-O bond in Se(VI) is stronger than that in Se(IV) and the first coordination shell of Se(VI) is more difficult to distort or disrupt compared to that of Se(IV) (Foster et al. 2003; Peak, 2006). As a result, the sorption of Se (VI) generally induced little isotope fractionation (Johnson and Bullen, 2004) in comparison with Se (IV) whose first coordination shell is more easily distorted. Changes in coordination have been identified as the cause of isotope fractionation during adsorption of several elements including Ge, Mo, W, and Cd (Goldberg et al., 2009; Li and Liu, 2010; Kashiwabara et al., 2011, 2017; Pokrovsky et al., 2014; Wasylenki et al., 2014). Recently, Bryan et al. (2015) also proposed that stronger and stiffer bonds generally cause smaller coordination numbers, and slight distortion of the Zn coordination geometry in the adsorbed complex could drive a small isotope effect. Therefore, coordination geometry of Se species likely controls the extent of Se isotope fractionation during adsorption.

In addition, the isotope fractionation may be related to the formation of surface complexations. As discussed in Section 4.1, Se (IV) prefers to form inner-sphere complexes with Fe and Mn oxides, while Se (VI) tends to form outer-

sphere complexes. Formation of inner sphere complexes has been proposed as a driver of isotope fractionation (Lemarchand et al., 2007; Li and Liu, 2010; Kashiwabara et al., 2011; Pokrovsky et al., 2014). Lemarchand et al. (2007) suggested that the boron isotope fractionation during boric acid adsorption onto Fe and Mn oxides was mainly attributed to the formation of inner-sphere complexes. Li and Liu (2010) used the bidentate corner-sharing surface complexes (inner-sphere) as the dominant surface structures to predict the Ge isotope fractionation (1.7‰) caused by Ge ($Ge(OH)_4$ or $GeO(OH)_3^-$) adsorption onto Fe(III)-oxyhydroxide surfaces; Pokrovsky et al. (2014) confirmed this prediction by experiment. Similarly, Kashiwabara et al. (2011) pointed out that the main reason for the significant Mo isotope fractionation during MoO_4^{2-} adsorption onto hematite and Mn oxides is that Mo dominantly formed inner-sphere complexes (edge-sharing octahedral) that were different from dissolved Mo species forming outer-sphere complexes (corner-sharing tetrahedral). Consequently, different Se species likely form different surface complexes (inner-sphere vs. outer-sphere), which further lead to different Se isotope fractionations.

4.3. The effect of adsorbents (Fe, Mn and Al oxides) on Se adsorption and isotope fractionation

In our experiments, adsorbents not only had an influence on the amount of Se adsorbed (hematite > alumina > manganese oxide) but also on Se isotope fractionation, especially for Se(IV) (Figs. 1 and 2). This may be related to the physicochemical properties of selected metal oxides, such as the point of zero charge (PZC) and the adsorption mechanism. Previous studies have shown that the PZC is 4.2–6.9 for hematite, 1.5–2.8 for MnO_2, and 8–9.5 for alumina. Thus, hematite and alumina surfaces mainly have positive charges while MnO_2 has negative charges at pH 5–8 (Peak, 2006; Kashiwabara et al., 2011). Se oxyanions have negative charges, and adsorption of them by hematite and alumina is likely via electrostatic attraction and surface complexation reaction, whereas adsorption by MnO_2 is mostly via surface complexation reactions (Kashiwabara et al., 2011). This likely resulted in Se adsorption capacity of MnO_2 being weaker than hematite and alumina (see Section 3.1).

Since Se(IV) adsorbed onto hematite and MnO_2 mainly formed inner-sphere complexes whereas Se(IV) adsorbed onto Al oxides formed a mixture of outer-sphere (predominant) and inner-sphere surface complexes (Table 3) (Duc et al. 2003; Foster et al. 2003; Peak and Sparks, 2002; Peak, 2006; Catalano et al., 2006b), the isotope fractionation of Se(IV) adsorbed by hematite (0.87‰) and MnO_2 (1.24‰ at pH = 5) was larger than that of aluminum oxides (0.08 ‰ for α-Al_2O_3 and 0.05‰ for γ-Al_2O_3). These phenomena have also been observed in isotope adsorption experiments with other elements such as B, Zn, Mo, and W (Pokrovsky et al., 2005; Lemarchand et al., 2005, 2007; Juillot et al., 2008; Goldberg et al., 2009; Kashiwabara et al. 2011, 2017). For instance, Kashiwabara et al. (2011) proposed that the proportion of octahedral (*Oh*) in Mo surface complexes (100% tetrahedron (*Td*) for ferrihydrite, 46% *Td* + 54% *Oh* for goethite, 14% *Td* + 86% *Oh* for hematite and 100% *Oh* for Mn oxides) is positively correlated with the magnitude of Mo isotope fractionation during MoO_4^{2-} adsorption onto Fe and Mn oxides: ferrihydrite (1.11‰) < goethite (1.40‰) < hematite (2.19‰) < birnessite (2.70‰) (Barling and Anbar, 2004; Wasylenki et al., 2008; Goldberg et al., 2009). This suggests that higher proportion of *Oh* (i.e. more distortion of Mo in surface complexes) leads to larger Mo isotope fractionation. In a similar fashion, we infer that the proportion of inner-sphere surface complex, or the magnitude of distortion in Se surface complexes during Se(IV) adsorption onto Fe, Mn, and Al oxides at pH 5 follows the descending order: MnO_2 > hematite > alumina.

Interestingly, Se(IV) adsorbed onto alumina didn't cause significant Se isotope fractionation at adsorption equilibrium, although the $\delta^{82/76}$Se of dissolved Se greatly changed during the initial period. One possible explanation for this early isotope fractionation is due to an initial kinetic isotope effects, which are subsequently overprinted by an equilibrium isotope effects (isotope exchange between adsorbed and dissolved Se) when adsorption reached equilibrium. Previous studies have shown that alumina are amphoteric compounds that may undergo hydrolysis or aging (Laiti et al., 1998; Wijnja and Schulthess, 2000; Peak, 2006). The hydroxyl-terminated alumina surface would be much less reactive toward water and the outermost surface would convert to a gibbsite/bayeritelike atomic arrangement, essentially passivating the surface (Eng et al., 2000). Catalano et al. (2006a) and Xu et al. (2018, 2019) revealed that the additional layering in the interfacial water gradually decays toward disordered bulk water away from the α-Al_2O_3 (0 1 2) surface. Hence, we conjectured that the final structure of Se (IV) adsorbed onto alumina (surface complexes) was similar to the structure of Se (IV) in solution when the adsorption reached equilibrium, resulting in little or no Se isotope fractionation.

4.4. The effect of pH on Se adsorption and isotope fractionation

Our results show that pH plays an important role in controlling the amount of Se(IV) adsorbed. Increasing pH decreases Se(IV) adsorption for all oxides invested in this study (Table 2), consistent with previous studies (Hayes, et al., 1987a, b; Kuan et al., 1998; Peak, 2006). On the one hand, the activity of hydroxide ion (OH^-) increases as pH increases, intensifying the competition for active surface sites on oxides among OH^- and SeO_3^{2-} or $HSeO_3^-$. On the other hand, the protonation efficiency of oxide surface decreases as pH increases (Duc et al., 2003, 2006). This would cause the number of positive charges on oxide surfaces to decrease, and thus leads to less Se(IV) adsorbed on the oxides via electrostatic attraction.

The pH effect on Se(IV) adsorption capacity is similar for Fe, Mn and Al oxides, but the pH effect for Se isotope fractionation varies for these oxides (Table 2). Since Se (VI) dominantly exists in the form of SeO_4^{2-} (close to 100%) at pH ≥ 3.5, pH should not have effects on Se(VI) protonation and thus isotope fractionation. The $\Delta^{82/76}Se_{dissolved\text{-}adsorbed}$

is also nearly non-responsive to the change of pH (5–8) during Se(IV) adsorption onto hematite and alumina (α- and γ-Al_2O_3). For Se(IV) adsorption to Mn oxide, however, the $\Delta^{82/76}Se_{dissolved\text{-}adsorbed}$ decreased from 1.24‰ at pH 5 to − 0.08‰ at pH 8. With a pKa close to 7, the Se speciation in Se(IV) (e.g., Na_2SeO_3) solution should change significantly from pH 5 to 8: Se(IV) switching from mostly protonated ($HSeO_3^-$, >95%) at pH = 6 to unprotonated (SeO_3^{2-}, ~50%) at pH 8 (Brookins,1988; Seby et al., 2001; Scott, 1991). Moreover, Li and Liu (2011) calculated that the equilibrium Se isotope fractionation between SeO_3^{2-} and $HSeO_3^-$ was only 0.5‰, with SeO_3^{2-} being isotopically heavier. Thus, protonation of Se(IV) (i.e., pH) alone cannot explain the range of observed $\Delta^{82/76}Se_{dissolved\text{-}adsorbed}$ during Se(IV) adsorption to MnO_2. The surface properties affected by pH must have led to the variation of Se isotope fractionation.

In addition, Se isotope fractionation may be related to Se oxidation occurring during Se(IV) adsorption onto β-MnO_2. However, we did not detect Se(VI) formation (detection limit of <0.1 ng/L), consistent with the findings in Balistrieri and Chao (1990). Studies have shown that the coordination number of anion species (e.g., Se(IV), U (VI)) adsorbed onto vernadite changed with pH; bidentate complexes dominate at low pH whereas monodentate complexes dominate at high pH (Foster et al., 2003; Wang et al., 2013). Additionally, the crystal structure of birnessite would change from hexagonal to triclinic with increasing pH (Ling et al., 2015). Vernadite and birnessite have layered structures, compared to β-MnO_2 that has a tunnel-type structure. However, all three share a Mn-O octahedra coordination (Post, 1999). This implies that these three minerals might have similar physicochemical properties. Therefore, the variation of the physicochemical properties of β-MnO_2 or the structures of surface complexes as a function of pH may contribute to the pH dependence of Se isotope fractionation during Se(IV) adsorption onto β-MnO_2. The observed pH dependence is very drastic: from a strong isotopic fractionation (i.e. requiring a distorted inner-sphere complex) at pH = 5.0, to a near-zero fractionation at pH = 8.0. We suggest that the absence of fractionation at pH 8 is caused by a change to either an outer-sphere adsorption mechanism or a new inner sphere complex that is less distorted than the lower-pH complex. Distinguishing these two scenarios is beyond the scope of this study, but could possibly be investigated by future EXAFS studies.

4.5. A model for Se isotope fractionation during adsorption

Mass dependent fractionation (MDF) could be due to either equilibrium isotope exchange processes or kinetic processes (e.g., Rayleigh model), or the combination of both (Young et al., 2002; Wasylenki et al., 2008). Recent studies reported that adsorption of Mo, W, Ge onto Fe and Mn oxides followed the equilibrium fractionation model and it was generally concluded that dissolved and adsorbed ions reached isotopic equilibrium relatively quickly (about 48 h) (Barling and Anbar, 2004; Wasylenki et al., 2008; Goldberg et al., 2009; Li and Liu, 2011; Kashiwabara et al., 2011, 2017). If Se isotope fractionation during adsorption were due to kinetic effect, the $\delta^{82/76}Se$ values should vary systematically as a function of the proportion of Se retained in solution, following a Rayleigh distillation model. We plotted the $\delta^{82/76}Se_{dissolved}$ values vs the percentage of Se remaining in solution f (Fig. 3), and found that the $\delta^{82/76}Se_{dissolved}$ values appear to follow the Rayleigh trend in the initial period (<1 h) when the forward reaction (adsorption) dominates. However, the $\delta^{82/76}Se_{dissolved}$ values deviated from the kinetic fractionation trend after a certain time point (1 h) when back-reaction (desorption) increases, eventually approaching the equilibrium fractionation line (Fig. 3).

This 2-step isotope fractionation was also observed for Cr adsorption onto goethite and alumina (Ellis, 2003). It was proposed that lighter isotopes preferentially diffuse from solution onto the mineral surface at a faster rate during the initial period, leading to an isotopically heavier solution. However, after a certain period (4 h or longer), the system eventually reached isotopic equilibrium, with small or no measurable isotope fractionation. In addition, Wasylenki et al. (2014) reported that Cd isotope fractionation briefly followed a Rayleigh model when Cd^{2+} was adsorbed onto birnessite at high ionic strength, but later deviated from the Rayleigh model due to isotope exchange between dissolved and adsorbed Cd. Therefore, we suggest that Se(IV) adsorption process includes an initial kinetic isotope fractionation step, followed by an equilibrium isotope fractionation step. In natural environments where the solution and solids may be in contact for several hours or more, the Se isotope fractionation caused by adsorption is best described using the equilibrium fractionation factor, whereas in rapidly changing systems (e.g., near surface zones subjected to major rainfall events) kinetic effects could produce greater fractionations.

4.6. Implications

Selenium isotopes can play important roles in tracing the migration of Se species, their biogeochemical cycling, continental weathering processes and reconstructing Se speciation and biogeochemistry in the oceans (Johnson et al., 1999, 2003; Herbel et al., 2000, 2002; Rouxel et al., 2002; Wen and Carignan et al., 2011; Mitchell et al., 2012, 2016; Zhu et al., 2014; Pogge von Strandmann et al., 2015; Stüeken et al., 2015a, 2017; Kipp et al., 2017). Previous studies have indicated that biological ($\varepsilon^{82/76}Se$ is 1.4–8‰ for Se(VI) to Se(IV) and 8–14‰ for Se(IV) to Se(0)) and abiotic reduction (8–18‰ and 9.8–20‰) usually cause significant Se isotope fractionations (Rees and Thode, 1966; Johnson et al., 1999; Johnson, 2004; Herbel et al., 2000; Ellis et al. 2003; Johnson and Bullen, 2003, Mitchell et al. 2013). In this study, we observed that Se (VI) adsorption onto Fe oxides causes approximately 0.2‰ equilibrium Se isotope fractionation, and insignificant fractionation with adsorption onto Mn and Al (α/γ) oxides. In contrast, Se (IV) adsorption onto Fe and Mn oxides can induce up to 0.87‰ and 1.24‰ equilibrium Se isotope fractionations ($\Delta^{82/76}Se_{dissolved\text{-}adsorbed}$), respectively, but with transient kinetic isotope fractionations ranging up to 3‰ (Fig. 2E). Previous studies reported 0.5–0.8‰ Se isotope fractionation

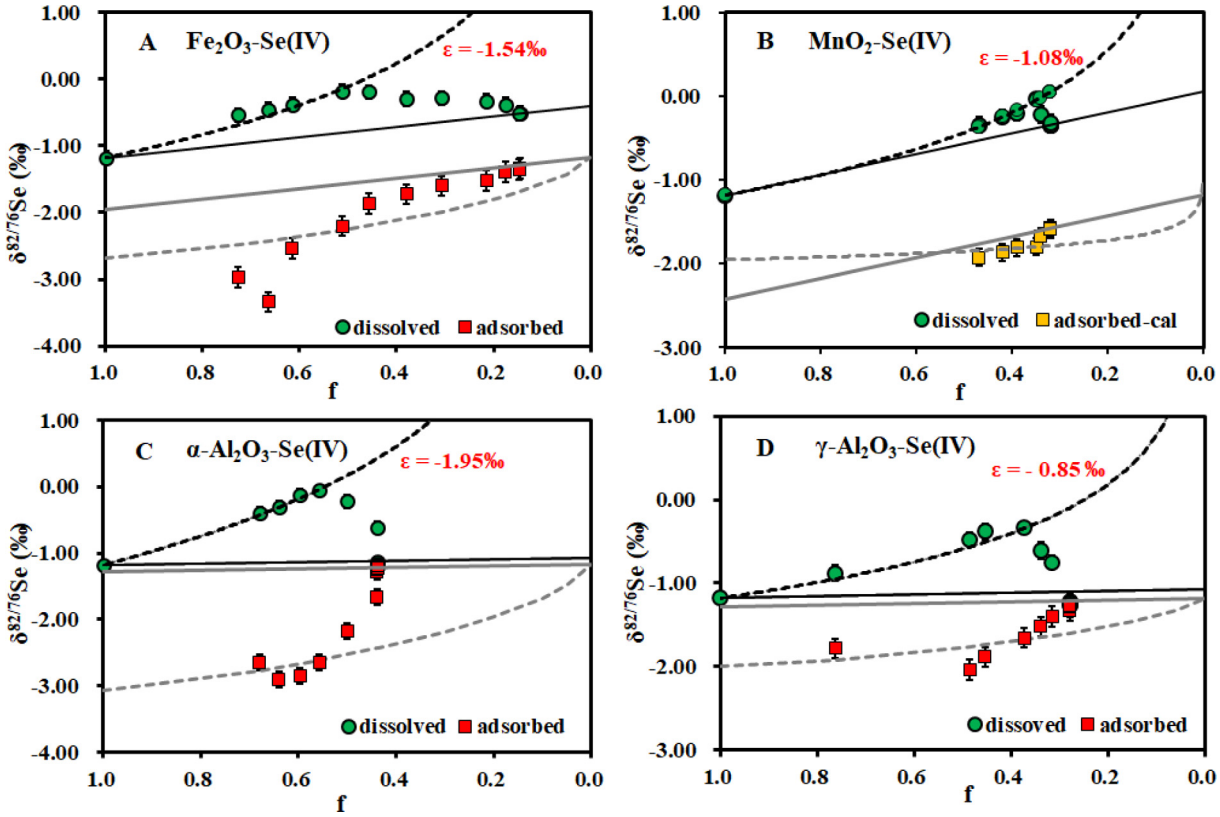

Fig. 3. The relationship between $\delta^{82/76}Se$ and the fraction of Se(IV) remaining in solution (f). Green filled circles represent measured $\delta^{82/76}Se_{dissolved}$; red square represents measured $\delta^{82/76}Se_{adsorbed,}$ yellow filled square represents calculated $\delta^{82/76}Se_{adsorbed}$ by mass balance. Black dash lines represent the Rayleigh fractionation dissolved, grey dash lines represent the Rayleigh fractionation adsorbed, black lines represent the closed system dissolved, grey lines represent closed system adsorbed. (For interpretation of the references to color in this figure legend, the reader is referred to the web version of this article.)

during adsorption of Se(IV) onto the goethite and Fe oxyhydroxides (HFO) (Johnson et al., 1999; Johnson, 2004; Mitchell et al. 2013), which is comparable to our values for hematite and δ-MnO_2. These results indicate that adsorption of Se onto Fe and Mn oxides, especially Fe oxides, together with Se reduction, plays significant roles in controlling Se isotope fractionation in the epigenetic environment. The varying Se isotopic fractionations obtained so far for different processes could help disentangle biogeochemical processes of Se and track its fate in natural environments.

In ferromanganese nodules, Se concentration can be up to 0.5 mg/kg (such as NOD-P-1), which is three orders of magnitude higher than the average Se concentration in seawater Se (0.08 μg/L) (Cutter and Bruland, 1984; Rouxel et al., 2002). Rouxel et al. (2002) reported an average $\delta^{82/76}Se$ of 0.36‰ for the Fe-Mn-nodule (NOD-P-1) collected at 4300 m in the Pacific Ocean. A recent study showed that the $\delta^{82/76}Se_{\sum(Se(IV),\ Se(VI))}$ of Northwestern Pacific Ocean seawater is 0.40 ± 0.05‰ ($n = 4$) under 800 m depth (Chang et al., 2017). Although Fe oxyhydroxides and δ-MnO_2 are the main components of ferromanganese nodules (Marcus et al., 2015), our experiments with hematite is still applicable because similar adsorption-related Se isotope fractionations between Fe oxyhydroxide and hematite as discussed in above. Since $\Delta^{82/76}Se_{dissolved\text{-}adsorbed}$ of Se (IV) adsorption onto MnO_2 ocean pH (~8) is ~0‰ (Table 2), meaning that MnO_2-related adsorption would not cause strong fractionation in the pH range expected for the oceans over time since the pH of seawater range from 6.5 to 8.2 over geological history (pH of local environments may differ from this) (Halevy and Bachan, 2017; Krissansen-Totton et al., 2018). Consequently, Se isotope fractionation during ferromanganese nodule formation should be controlled by Se adsorption to Fe oxides ($\Delta^{82/76}Se_{seawater\text{-}adsorbed} \leq 0.5$–0.8‰). However, there is no significant difference between Northwestern Pacific seawater and NOD-P-1 (Rouxel et al., 2002; Change et al., 2017). Lack of Se isotope differences between modern seawater and nodules may be due to the fact that the majority of Se in seawater is Se(VI) and Se(VI) adsorption to both Mn and Fe oxides induce little or no Se isotope fractionations (Fig. 2B, D and J). Regardless of the underlying Se isotope fractionation mechanism during Fe-Mn nodule/crust formation, deep-sea ferromanganese nodules appear to record the Se isotope composition of deep seawater. More species-specific Se isotope composition data of modern seawater and Fe-Mn nodule/crust are needed to test this idea.

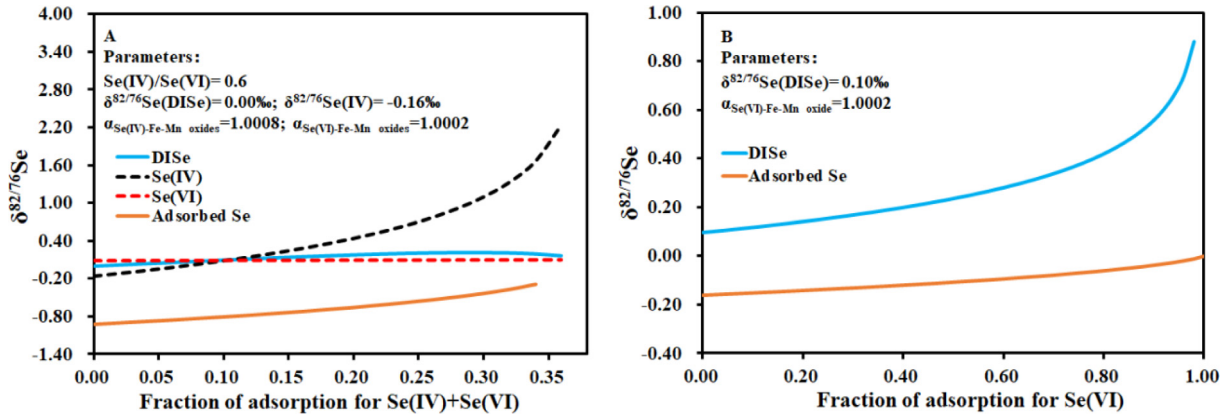

Fig. 4. A simple mass balance model illustrating the effects of Se adsorption onto Fe-Mn oxides on seawater $\delta^{82/76}Se_{adsorbed}$ evolution (DISe = Σ(Se(IV) + Se(VI)), which is the total dissolved inorganic Se in seawater). A. The Rayleigh model for adsorption of DISe by Fe-Mn Oxides; B. The Rayleigh model for adsorption of Se(VI) in seawater by Fe-Mn Oxides.

Several factors may have caused seawater $\delta^{82/76}Se$ to be positive. First, Se (IV) is easily absorbed onto particulates, which has two consequences: (1) leaving residual Se(IV) isotopically heavy, and (2) making Se(VI) the predominant species in most rivers (Clark and Johnson, 2010; Chang, 2017) and thus the ocean, since rivers are the most important input of Se to the ocean (Stüeken et al., 2017). In addition, partial oxidation of Se (IV) to Se (VI) also enriches heavy isotopes in Se(VI) (Schilling et al., 2015). These two effects lead to isotopically heavy dissolved Se in rivers and the ocean. Indeed, the reported $\delta^{82/76}Se$ values of the Yangtze River and Uncompahgre River are $1.29 \pm 0.29‰$ (n = 12) and $2.95 \pm 0.23‰$ (n = 9) (Clark and Johnson, 2010; Chang, 2017).

In order to explore the effect of Se adsorption onto Fe-Mn oxide on sweater $\delta^{82/76}Se$ evolution, we constructed a simple mass balance model (Fig. 4). Several assumptions are made: (1) Se isotopes are at a steady state (only equilibrium isotope fractionation is considered); (2) seawater Se (IV)/Se(VI) is 0.4 (Chang et al, 2017; Mason et al., 2018); (3) seawater $\delta^{82/76}Se(IV)$ starts at −0.16‰ (Yierpan et al., 2019) and seawater $\delta^{82/76}Se(total)$ starts at 0‰ (Fig. 4A); (4) during Se adsorption to a mixture of Fe and Mn oxides, $\Delta^{82/76}Se(IV)_{dissolved\text{-}adsorbed} = 0.8‰$ and $\Delta^{82/76}Se(VI)_{dissolved\text{-}adsorbed} = 0.2‰$; (5) during adsorption the Se(IV)/Se(VI) ratio gradually approaches zero with time (Fig. 4B). According to the model, as the amount of adsorbed Se doubles, seawater $\delta^{82/76}Se$ changes by 0.44‰ (f = 0.8 in Fig. 4B). Therefore, during red bed and banded iron formation deposition, which primarily occurred between 3.0 Ga and 2.5 Ga and right before the GOE (Bekker et al., 2010; Gumsley et al., 2017), seawater $\delta^{82/76}Se$ could have experienced positive excursions as recorded in offshore shales (Kipp et al., 2017). Thus, the evolution of Se isotopes in seawater should be re-examined given the influence of Se adsorption onto iron and manganese oxides.

5. CONCLUSIONS

This study reports for the first time Se isotope fractionation during adsorption of Se(VI) and Se(IV) onto alumina and Mn oxide, and re-examines Se isotope fractionation during Se(VI) and Se(IV) adsorption onto hematite. There are significant Se isotopic fractionations during Se(IV) adsorption onto Fe, Mn oxides, with lighter isotopes preferentially adsorbed. At pH 5, Se(IV) adsorbed onto hematite and MnO_2 induces 0.87‰ and 1.24‰ fractionations, respectively. For Se(VI) adsorption, however, Se isotope fractionation was less than 0.2‰ for all oxides investigated.

By contrast, Se oxyanions adsorption onto alumina (α and γ-Al_2O_3) does not induce significant Se isotope fractionation (<0.2‰) after isotopic equilibrium is approached, despite transient kinetic effects that caused the $\delta^{82/76}Se$ of dissolved Se to change greatly in the early stages of the experiments. The large difference in isotopic fractionation between the alumina and Fe or Mn oxides experiments indicates that the magnitude of isotope fractionation is related to the types of absorbent, and the structures of surface complexes formed between Se and the oxide surfaces.

pH has a very small influence on Se isotope fractionation during Se(IV) adsorption onto hematite and alumina, but has a great influence on Se(IV) adsorption onto MnO_2, with $\Delta^{82/76}Se_{dissolved\text{-}adsorbed}$ decreasing from 1.24‰ at pH 5 to −0.08 ‰ at pH 8. This is likely due to changes in physicochemical properties of manganese oxide and/or the structures of surface complexes as pH changes. These results may help us interpret the Se isotope composition in ferromanganese crusts as a proxy of the evolution of Se isotopes in the oceans through time.

Declaration of Competing Interest

The authors declare that they have no known competing financial interests or personal relationships that could have appeared to influence the work reported in this paper.

ACKNOWLEDGEMENTS

This study was financially supported by the National Natural Science Foundation of China (No. 41273029, U1612441 and 41473028). The authors thank Dr. Liang Liang, Zhuo Lu and Kai Lu for their assistance with the sample preparation, Dr. Jing

Wang and Dr. Li Zeng for assistance with mass spectrometry and Dr. Qi Liu for the discussion of this paper. The authors also appreciate the constructive comments and insightful suggestions of Bleuenn Guéguen and other two anonymous reviewers, and Drs. Jeffrey G. Catalano and Olivier Rouxel for editorial handling.

APPENDIX A. SUPPLEMENTARY MATERIAL

Supplementary data to this article can be found online at https://doi.org/10.1016/j.gca.2020.01.001.

REFERENCES

Balistrieri L. S. and Chao T. T. (1990) Adsorption of selenium by amorphous iron oxyhydroxide and manganese dioxide. *Geochim. Cosmochim. Acta* **54**, 739–751.

Barling J. and Anbar A. D. (2004) Molybdenum isotope fractionation during adsorption by manganese oxides. *Earth Planet. Sci. Lett.* **217**, 315–329.

Bekker A., Slack J. F., Planavsky B., Krapež B., Hofmann A., Konhauser K. O. and Rouxel O. J. (2010) Iron formation: the sedimentary product of a complex interplay among mantle, tectonic, oceanic, and biospheric processes. *Econ. Geol.* **105**, 467–508.

Bryan A. L., Dong S., Wilkes E. B. and Wasylenki L. E. (2015) Zinc isotope fractionation during adsorption onto Mn oxyhydroxide at low and high ionic strength. *Geochim. Cosmochim. Acta* **157**, 182–197.

Brookins D. G. (1988) *Eh- pH Diagrams for Geochemistry*. Springer-Verlag, Berlin, pp. 18–19.

Catalano J. G., Park C., Zhang Z. and Fenter P. (2006a) Termination and water adsorption at the α-Al_2O_3 (012)-aqueous solution interface. *Langmuir* **22**, 4668–4673.

Catalano J. G., Zhang Z., Fenter P. and Bedzyk M. J. (2006b) Inner-sphere adsorption geometry of Se(IV) at the hematite (100)-water interface. *J. Colloid Interface Sci.* **297**, 665–671.

Chang Y. (2017) *Biogeochemical Processes of Dissolved Selenium and Isotopes in the Coastal Areas* Ph.D. thesis. East China Normal University, Shanghai, China.

Chang Y., Zhang J., Qu J.-Q. and Xue Y. (2017) Precise selenium isotope measurement in seawater by carbon-containing hydride generation-Desolvation-MC-ICP-MS after thiol resin preconcentration. *Chem. Geol.* **471**, 65–73.

Clark S. K. and Johnson T. M. (2008) Effective isotopic fractionation factors for solute removal by reactive sediments a laboratory microcosm and Slurry Study. *Environ. Sci. Technol.* **42**, 7850–7855.

Clark S. K. and Johnson T. M. (2010) Selenium stable isotope investigation into selenium biogeochemical cycling in a lacustrine environment: Sweitzer Lake, Colorado. *J. Environ. Qual.* **39**, 2200–2210.

Cutter G. A. and Bruland K. W. (1984) The marine biogeochemistry of selenium: a re-evaluation. *Limnol. Oceanogr.* **29**, 1179–1192.

Dowdle P. R. and Oremland R. S. (1998) Microbial oxidation of elemental selenium in soil slurries and bacterial cultures. *Environ. Sci. Technol.* **32**, 3749–3755.

Duc M., Lefevre G. and Fedoroff M. (2006) Sorption of selenite ions on hematite. *J. Colloid Interface Sci.* **298**, 556–563.

Duc M., Lefevre G., Fedoroff M., Jeanjean J., Rouchaud J. C., Monteil-Rivera F., Dumonceau J. and Milonjic S. (2003) Sorption of selenium anionic species on apatites and iron oxides from aqueous solutions. *J. Environ. Radioactiv.* **70**, 61–72.

Ellis A. S., Johnson T. M., Herbel M. J. and Bullen T. D. (2003) Stable isotope fractionation of selenium by natural microbial consortia. *Chem. Geol.* **195**, 119–129.

Ellis A. (2003) *Selenium and chromium stable isotopes and the fate of redox-active contaminants in the environment* Ph.D. thesis. The University of Illinois at Urbana-Champain, Urbana, Illinois.

Elrashidi M. A., Adriano D. C., Workman S. M. and Lindsay W. L. (1987) Chemical equilibria of selenium in soils. *Soil Sci.* **144**, 141–152.

Eng P. J., Trainor T. P., Brown G. E., Waychunas G. A., Newville M., Sutton S. R. and Rivers M. L. (2000) Structure of the hydrated -Al_2O_3 (0001) surface. *Science* **288**, 1029–1033.

Foster A. L., Brown G. E. and Parks G. A. (2003) X-ray absorption fine structure study of As(V) and Se(IV) sorption complexes on hydrous Mn oxides. *Geochim. Cosmochim. Acta* **67**, 1937–1953.

Goldberg T., Archer C., Vance D. and Poulton S. W. (2009) Mo isotope fractionation during adsorption to Fe (oxyhydr)oxides. *Geochim. Cosmochim. Acta* **73**, 6502–6516.

Gueguen B., Sorensen J. V., Lalonde S. V., Peña J. T., Brandy M. and Rouxel O. (2018) Variable Ni isotope fractionation between Fe-oxyhydroxides and implications for the use of Ni isotopes as geochemical tracers. *Chem. Geol.* **481**, 38–52.

Gumsley A. P., Chamberlain K. R., Bleeker W., Söderlund U., De Kock M. O., Larsson E. R. and Bekker A. (2017) Timing and tempo of the great oxidation event. *Proc. Natl. Acad. Sci. USA* **114**(8), 1811–1816.

Halevy I. and Bachan A. (2017) The geologic history of seawater pH. *Science* **335**, 1069–1071.

Hayes K. F., Papelis C. and Leckie J. O. (1987a) Modeling ionic strength effects on anion adsorption at hydrous oxide/solution interfaces. *J. Colloid Interface Sci.* **125**, 717–726.

Hayes K. F., Roe A. L., Brown G. E., Hodgson K. O., Leckie J. O. and Parks G. A. (1987b) In situ X-ray absorption study of surface complexes selenium oxyanions on α-FeOOH. *Science* **238**, 783–786.

Herbel M. J., Johnson T. M., Oremland R. S. and Bullen T. D. (2000) Fractionation of selenium isotopes during bacterial respiratory reduction of selenium oxyanions. *Geochim. Cosmochim. Acta* **64**, 3701–3709.

Herbel M. J., Johnson T. M., Tanji K. K., Gao S. and Bullen T. D. (2002) Selenium stable isotope ratios in California agricultural drainage water management systems. *J. Environ. Qual.* **31**, 1146–1156.

Johnson T. M. (2004) A review of mass-dependent fractionation of selenium isotopes and implications for other heavy stable isotopes. *Chem. Geol.* **204**, 201–214.

Johnson T. M. and Bullen T. D. (2003) Selenium isotope fractionation during reduction by Fe(II)-Fe(III) hydroxide-sulfate (green rust). *Geochim. Cosmochim. Acta* **67**, 413–419.

Johnson T. M. and Bullen T. D. (2004) Mass-dependent fractionation of selenium and chromium isotopes in low-temperature environments. *Rev. Mineral Geochem.* **55**, 289–317.

Johnson T. M., Bullen T. D. and Zawislanski P. T. (2000) Selenium stable isotope ratios as indicators of sources and cycling of selenium results from the northern reach of San Francisco bay. *Environ. Sci. Technol.* **34**, 2075–2079.

Johnson T. M., Herbel M. J. and Bullen T. D. (1999) Selenium isotope ratios as indicators of selenium sources and oxyanion reduction. *Geochim. Cosmochim. Acta* **63**(18), 2775–2783.

Juillot F., Marechal C., Ponthieu M., Cacaly S., Morin G., Benedetti M., Hazemann J. L., Proux O. and Guyot F. (2008) Zn isotopic fractionation caused by sorption on goethite and 2-Lines ferrihydrite. *Geochim. Cosmochim. Acta* **72**, 4886–4900.

Kashiwabara T., Kubo S., Tanaka M., Senda R., Iizuka T., Tanimizu M. and Takahashi Y. (2017) Stable isotope

fractionation of tungsten during adsorption on Fe and Mn (oxyhydr)oxides. *Geochim. Cosmochim. Acta* **204**, 52–67.

Kashiwabara T., Takahashi Y. and Tanimizu M. (2009) A XAFS study on the mechanism of isotopic fractionation of molybdenum during its adsorption on ferromanganese oxides. *Geochem. J.* **43**, 31–36.

Kashiwabara T., Takahashi Y., Tanimizu M. and Usui A. (2011) Molecular-scale mechanisms of distribution and isotopic fractionation of molybdenum between seawater and ferromanganese oxides. *Geochim. Cosmochim. Acta* **75**, 5762–5784.

Kipp M. A., Stueken E. E., Bekker A. and Buick R. (2017) Selenium isotopes record extensive marine suboxia during the Great Oxidation Event. *Proc. Natl. Acad. Sci. USA* **114**, 875–880.

Krissansen-Totton J., Arney G. N. and Catling D. C. (2018) Constraining the climate and ocean pH of the early Earth with a geological carbon cycle model. *Proc. Natl. Acad. Sci. USA* **115**, 4105–4110.

Kuan W.-H., Lo S.-L., Wang M. K. and Lin C.-F. (1998) Removal of Se(IV) and Se(VI) from water by aluminum-oxide-coated sand. *Wat. Res.* **32**, 915–923.

Laiti E., Persson P. and Ohman L.-O. (1998) Balance between surface complexation and surface phase transformation at the alumina/water interface. *Langmuir* **14**, 825–831.

Lemarchand E., Schott J. and Gaillardet J. (2005) Boron isotopic fractionation related to boron sorption on humic acid and the structure of surface complexes formed. *Geochim. Cosmochim. Acta* **69**, 3519–3533.

Lemarchand E., Schott J. and Gaillardet J. (2007) How surface complexes impact boron isotope fractionation: evidence from Fe and Mn oxides sorption experiments. *Earth Planet. Sci. Lett.* **260**, 277–296.

Li X. and Liu Y. (2011) Equilibrium Se isotope fractionation parameters: a first-principles study. *Earth Planet. Sci. Lett.* **304**, 113–120.

Li X. F. and Liu Y. (2010) First-principles study of Ge isotope fractionation during adsorption on Fe(III)-oxyhydroxide surfaces. *Chem. Geol.* **278**, 15–22.

Ling F. T., Heaney P. J., Post J. E. and Gao X. (2015) Transformations from triclinic to hexagonal birnessite at circumneutral pH induced through pH control by common biological buffers. *Chem. Geol.* **416**, 1–10.

Liu J. J., Zheng M. H., Liu J. M. and Su W. C. (2000) Geochemistry of the La'erma and Qiongmo Au–Se deposits in the western Qinling Mountains, China. *Ore Geol. Rev.* **17**, 91–111.

Manceau A. and Charlet L. (1994) The mechanism of selenate adsorption on goethite and hydrous ferric oxide. *J. Colloid Interface Sci.* **168**, 87–93.

Marcus M. A., Edwards K. J., Gueguen B., Fakra S. C., Horn G., Jelinski N. A., Rouxel O., Sorensen J. and Toner B. M. (2015) Iron mineral structure, reactivity, and isotopic composition in a South Pacific Gyre ferromanganese nodule over 4 Ma. *Geochim. Cosmochim. Acta* **171**, 61–79.

Mason R. P., Soerensen A. L., DiMento B. P. and Balcom P. H. (2018) The global marine selenium cycle: insights from measurements and modeling. *Global Biogeochem. Cy.* **32**, 1720–1737.

McNeal J. M. and Balistrieri L. S. (1989) Geochemistry and occurrence of selenium; an overview. In *Selenium in Agriculture and the Environment. SSSA Special Publication* (ed. L. W. Jacobs). Soil Science Society of America, Madison, WI, pp. 1–13.

Mitchell K., Couture R.-M., Johnson T. M., Mason P. R. D. and Van Cappellen P. (2013) Selenium sorption and isotope fractionation: Iron(III) oxides versus iron(II) sulfides. *Chem. Geol.* **342**, 21–28.

Mitchell K., Mansoor S. Z., Mason P. R. D., Johnson T. M. and Van Cappellen P. (2016) Geological evolution of the marine selenium cycle: insights from the bulk shale $\delta^{82/76}$Se record and isotope mass balance modeling. *Earth Planet. Sci. Lett.* **441**, 178–187.

Mitchell K., Mason P. R. D., Van Cappellen P., Johnson T. M., Gill B. C., Owens J. D., Diaz J., Ingall E. D., Reichart G.-J. and Lyons T. W. (2012) Selenium as paleo-oceanographic proxy: a first assessment. *Geochim. Cosmochim. Acta* **89**, 302–317.

Peak D. (2006) Adsorption mechanisms of selenium oxyanions at the aluminum oxide/water interface. *J. Colloid Interface Sci.* **303**, 337–345.

Peak D., Saha U. K. and Huang P. M. (2006) Selenite adsorption mechanisms on pure and coated montmorillonite: an EXAFS and XANES spectroscopic study. *Soil Sci. Soc. Am. J.* **70**, 192–203.

Peak D. and Sparks D. L. (2002) Mechanisms of selenate adsorption on iron oxides and hydroxides. *Environ. Sci. Technol.* **36**, 1460–1466.

Pogge von Strandmann P. A. E., Stüeken E. E., Elliott T., Poulton S. W., Dehler C. M., Canfield D. E. and Catling D. C. (2015) Selenium isotope evidence for progressive oxidation of the Neoproterozoic biosphere. *Nat. Commun.* **6**, 1–10.

Pokrovsky O. S., Galy A., Schott J., Pokrovski G. S. and Mantoura S. (2014) Germanium isotope fractionation during Ge adsorption on goethite and its coprecipitation with Fe oxy(hydr)oxides. *Geochim. Cosmochim. Acta* **131**, 138–149.

Pokrovsky O. S., Viers J. and Freydier R. (2005) Zinc stable isotope fractionation during its adsorption on oxides and hydroxides. *J. Colloid Interface Sci.* **291**, 192–200.

Post J. E. (1999) Manganese oxide minerals: Crystal structures and economic and environmental significance. *Proc. Natl. Acad. Sci. USA* **96**, 3447–3454.

Rayman M. P. (2000) The importance of selenium to human health. *Lancet* **356**, 233–241.

Rees C. B. and Thode H. G. (1966) Selenium isotope effects in the reduction of sodium selenite and of sodium selenate. *Can. J. Chem.* **44**, 419–427.

Rouxel O., Ludden J., Carignan J., Marin L. and Fouquet Y. (2002) Natural variations of Se isotopic composition determined by hydride generation multiple collector inductively coupled plasma mass spectrometry. *Geochim. Cosmochim. Acta* **66**, 3191–3199.

Rovira M., Gimenez J., Martinez M., Martinez-Llado X., de Pablo J., Marti V. and Duro L. (2008) Sorption of selenium(IV) and selenium(VI) onto natural iron oxides: goethite and hematite. *J. Hazard. Mater.* **150**, 279–284.

Saeki K. and Matsumoto S. (1994) Selenite adsorption by a variety of oxides. *Commun. Soil Sci. Plan.* **25**, 2147–2158.

Saeki K., Matsumoto S. and Tatsukawa R. (1995) Selenite adsorption by manganese oxides. *Soil Sci.* **160**, 265–272.

Scott M. J. (1991) *Kinetics of adsorption and redox processes on iron and manganese oxides: Reactions of As(III) and Se(IV) at goethite and birnessite surfaces* Ph.D. thesis. California Institute of Technology, California.

Seby F., Potin-Gautier M., Giffaut E., Borge G. and Donard O. F. X. (2001) A critical review of thermodynamic data for selenium species at 25 . *Chem. Geol.* **171**, 171–194.

Schilling K., Johnson T. M., Dhillon K. S. and Mason P. R. D. (2015) Fate of selenium in soils at a seleniferous site recorded by high precision Se isotope measurements. *Environ. Sci. Technol.* **49**(16), 9690–9698.

Simon G., Kesler S. E. and Essene E. J. (1997) Phase relations among selenides, sulfides, tellurides and oxides: II. applications to selenides-bearing ore deposits. *Econ. Geol.* **92**, 468–484.

Stüeken E. E. (2017) Selenium isotopes as a biogeochemical proxy in deep time. *Rev. Mineral Geochem.* **82**, 657–682.

Stüeken E. E., Buick R. and Anbar A. D. (2015a) Selenium isotopes support free O_2 in the latest Archean. *Geology* **43**, 259–262.

Stüeken E. E., Buick R., Bekker A., Catling D., Foriel J., Guy B. M., Kah L. C., Machel H. G., Montañez I. P. and Poulton S. W. (2015b) The evolution of the global selenium cycle: secular trends in Se isotopes and abundances. *Geochim. Cosmochim. Acta* **162**, 109–125.

Stüeken E. E., Foriel J., Buick R. and Schoepfer S. D. (2015c) Selenium isotope ratios, redox changes and biological productivity across the end-Permian mass extinction. *Chem. Geol.* **410**, 28–39.

Wang Z., Lee S. W., Catalano J. G., Lezama-Pacheco J. S., Bargar J. R., Tebo B. M. and Giammar D. E. (2013) Adsorption of uranium(VI) to manganese oxides: X-ray absorption spectroscopy and surface complexation modeling. *Environ Sci. Technol.* **47**, 850–858.

Wasylenki L. E., Rolfe B. A., Weeks C. L., Spiro T. G. and Anbar A. D. (2008) Experimental investigation of the effects of temperature and ionic strength on Mo isotope fractionation during adsorption to manganese oxides. *Geochim. Cosmochim. Acta* **72**, 5997–6005.

Wasylenki L. E., Swihart J. W. and Romaniello S. J. (2014) Cadmium isotope fractionation during adsorption to Mn oxyhydroxide at low and high ionic strength. *Geochim. Cosmochim. Acta* **140**, 212–226.

Wasylenki L. E., Weeks C. L., Bargar J. R., Spiro T. G., Hein J. R. and Anbar A. D. (2011) The molecular mechanism of Mo isotope fractionation during adsorption to birnessite. *Geochim. Cosmochim. Acta* **75**, 5019–5031.

Wen H. and Carignan J. (2011) Selenium isotopes trace the source and redox processes in the black shale-hosted Se-rich deposits in China. *Geochim. Cosmochim. Acta* **75**, 1411–1427.

World Health Organization (WHO) (1987) Environmental Health Criteria 58: Selenium Environmental Health Criteria. Geneva, pp. 1–110.

Wijnja H. and Schulthess C. P. (2000) Vibrational spectroscopy study of selenate and sulfate adsorption mechanisms on Fe and Al (Hydr)oxide surfaces. *J. Colloid Interface Sci.* **229**, 286–297.

Xu T., Stubbs J. E., Eng P. J. and Catalano J. G. (2018) Response of interfacial water to arsenate adsorption on corundum (0 0 1) surfaces: effects of pH and adsorbate surface coverage. *Geochim. Cosmochim. Acta* **239**, 198–212.

Xu T., Stubbs J. E., Eng P. J. and Catalano J. G. (2019) Comparative response of interfacial water structure to pH variations and arsenate adsorption on corundum (012) and (001) surfaces. *Geochim. Cosmochim. Acta* **246**, 406–418.

Yierpan A., Konig S., Labidi J. and Schoenberg R. (2019) Selenium isotope and S-Se-Te elemental systematics along the Pacific-Antarctic ridge Role of mantle processes. *Geochim. Cosmochim. Acta* **249**, 199–224.

Young E. D., Galy A. and Nagahara H. (2002) Kinetic and equilibrium mass-dependent isotope fractionation laws in nature and their geochemical and cosmochemical significance. *Geochim. Cosmochim. Acta* **66**, 1095–1104.

Zhang P. and Sparks D. L. (1990) Kinetics of selenate and selenite adsorption desorption at the goethite water interface. *Environ. Sci. Technol.* **24**, 1848–1856.

Zhu J.-M., Johnson T. M., Clark S. K. and Zhu X. K. (2008) High precision measurement of selenium isotopic composition by hydride generation multiple collector inductively coupled plasma mass spectrometry with a ^{74}Se-^{77}Se double spike. *Chinese J. Anal. Chem.* **36**, 1385–1390.

Zhu J.-M., Johnson T. M., Clark S. K., Zhu X.-K. and Wang X.-L. (2014) Selenium redox cycling during weathering of Se-rich shales: a selenium isotope study. *Geochim. Cosmochim. Acta* **126**, 228–249.

Zhu J.-M., Johnson T. M., Finkelman R. B., Zheng B. S., Sykorova I. and Pesek J. (2012) The occurrence and origin of selenium minerals in Se-rich stone coals, spoils and their adjacent soils in Yutangba, China. *Chem. Geol.* **330–331**, 27–38.

Zhu J.-M., Zuo W., Liang X. B., Li S. H. and Zheng B. S. (2004) Occurrence of native selenium in Yutangba and its environmental implications. *Appl. Geochem.* **19**, 461–467.

Associate Editor: Olivier J. Rouxel